Exploring growth kinetics of carbon nanotube arrays by *in situ* optical diagnostics and modeling

A. A. Puretzky, D. B. Geohegan, S. Pannala, C. M. Rouleau
Oak Ridge National Laboratory, Oak Ridge TN 37831, USA

ABSTRACT

Simple kinetic models of carbon nanotube growth have been able to successfully link together many experimental parameters involved in the growth of carbon nanotubes for practical applications including the prediction of growth rates, terminal lengths, number of walls, activation energies, and their dependences on the growth environment. The implications of recent experiments utilizing *in situ* monitoring of carbon nanotube growth on our past kinetic model are first reviewed. Then, sub-second pulsed feedstock gas introduction is discussed to explore the nucleation and initial growth of carbon nanotubes in the context of the kinetic model. Moreover, kinetic effects in "pulsed CVD" - using repeated pulsed gas introduction to stop and restart nanotube growth - are explored to understand renucleation, the origin of alignment in nanotube arrays, and incremental growth. Time-resolved reflectivity of the surface is used to remotely understand the kinetics of nucleation and the coordinated growth of arrays. This approach demonstrates that continuous vertically aligned single wall carbon nanotubes can be grown incrementally by pulsed CVD, and that the first exposure of fresh catalyst to feedstock gas is critical to nanotubes site density required for coordinated growth. Aligned nanotube arrays (as short as 60 nm) are shown to nucleate and grow within single, sub-second gas pulses. The multiple-pulse growth experiments (> 100 pulses) show that a high fraction of nanotubes renucleate on subsequent gas pulses.

Keywords: Carbon nanotubes, vertically aligned carbon nanotube arrays, chemical vapor deposition, growth kinetics, *in situ* diagnostics.

1. INTRODUCTION

Thin metal catalyst films were employed for successful growth of carbon nanotubes and graphene using chemical vapor deposition (CVD). In both cases metals with high (e.g., Fe, Ni, Co) and low (e.g., Cu) carbon solubility can be used, and the CVD growth procedures are similar except for the thicknesses of the metal films. More specifically, very thin metal catalyst films (~1 nm) are typically used for growth of carbon nanotubes and their arrays by dewetting the films upon heating to elevated temperatures and converting them into nanoparticles. Graphene, on the other hand, requires thick metal films (> 100 nm) to prevent dewetting during annealing and growth. Conceptually, graphene growth on metals should be very much like the initial stage of carbon nanotube growth - i.e., nanotube cap formation - and in both cases the key to understanding the growth mechanisms of these structures is the combination of *in situ* diagnostics and modeling. These techniques have been used extensively in the case of carbon nanotube synthesis, but are only now just beginning to be applied in graphene growth. Here we give an example of how *in situ* diagnostics and modeling help in understanding and optimization of the growth of vertically aligned carbon nanotube arrays (VANTAs), and how these approaches can also be applied to graphene synthesis as we have shown in a recent paper.[1]

Growth of VANTAs is based on the cooperative response of a large number of catalyst nanoparticles having different diameters and catalytic activities. Some fraction of these nanoparticles is able to maintain growth for a very long time, depending on the growth conditions. However, the mechanism of the cooperative growth is not understood yet, despite the volume of work in this area. To move further in the understanding of the cooperative growth of VANTAs, *in situ* diagnostics capable of monitoring the collective growth kinetics combined with modeling of the kinetics are required. Such an approach would allow one to study the collective response of an ensemble of different catalyst nanoparticles to rapid changes in the growth environment, e.g., rapid pulsed heating or fast pulsed feedstock gas introduction.

Recently, many different techniques for *in situ* monitoring of carbon nanotubes growth have been developed. The majority of these approaches were based on optical monitoring of the growth process, including time resolved reflectivity (TRR),[2-5] absorbance,[6-8] Raman scattering,[9-12] direct video imaging of growth process.[13-15] Considerable

Synthesis and Photonics of Nanoscale Materials XI, edited by David B. Geohegan, Frank Träger, Jan J. Dubowski,
Proc. of SPIE Vol. 8969, 896904 · © 2014 SPIE · CCC code: 0277-786X/14/$18 · doi: 10.1117/12.2045949

progress in our understanding of atomic-scale processes has been achieved, using environmental high resolution transmission electron microscopy HR-TEM,[16-25] and it was well established that a catalyst nanoparticle changes its shape during nucleation and growth and that in the case of Fe nanoparticles growth occurs from solid Fe_3C phase.[23,24] Although, atomic scale dignostics and modeling are very important for understanding of the growth mechanisms of carbon nanotubes, real-time optical monitoring combined with kinetic modeling is also necessary to link together numerous experimental parameters involved in the growth of carbon nanotubes and VANTAs for practical applications. It is also important to predict growth rates, terminal lengths, number of walls, activation energies, etc. and their dependences on growth environment.

2. KINETIC GROWTH MODEL

Our model has been developed to explain the experimental results observed in VANTAs growth and derived from *in situ* monitoring using time-resolved optical reflectivity. These results include 1) the time dependences of VANTA length, 2) growth rates and their temperature dependences, 3) observed growth termination both at low and high temperatures, 4) feedstock gas pressure dependence of the growth rate, and 5) temperature dependence of the number of walls. The model was based on the concept first discussed by Baker[26] and later used by many other researchers[27-29] to explain growth of both nanofibers and nanotubes. In this concept a carbon feedstock, e.g., acetylene, dissociates on a catalyst nanoparticle surface and the atomic carbon diffuses into and through the bulk and along the surface of the nanoparticle to the sites where a nanotube grows. Following this concept we introduced a constant incident molecular flux of carbon-containing molecules, F_{b1}, to the surface of a catalyst nanoparticle[4]

$$F_{b1} = 0.25 S_0 n (k_B T / 2\pi m)^{1/2}. \quad (1)$$

A small fraction of these molecules

$$F_{c1} = F_{b1} p_1 \exp(-E_{a1}/k_B T), \quad (2)$$

sticks to the nanoparticle surface and catalytically decomposes, producing carbon atoms for nanotube growth. Here S_0 is the surface area of the nanoparticle, n is the partial density of feedstock molecules in the gas flux, k_B is the Boltzmann constant, T is the temperature, m is the mass of a feedstock gas molecule, p_1 contains the sticking coefficient, geometric factors, etc., and E_{a1} is the activation energy for catalytic decomposition of the feedstock molecules. The majority of the carbon atoms diffuses to the nanotube precipitation sites and feeds the growth, but a relatively small fraction of these atoms forms a "carbonaceous" layer on the surface of the catalyst nanoparticle, which decreases the number of active sites or in other words nanoparticle surface area available for catalytic decomposition of the incoming feedstock molecules. As a result the source flux of carbon atoms available for the CNT growth will be restricted and finally, when the whole surface of the catalyst nanoparticle is "poisoned" by the carbonaceous layer, the source of carbon atoms terminates and the growth stops. The analytical solution of the corresponding rate equations (see Ref. 4) describing these processes gives the following expression for the time dependence of CNT length

$$L(t) = L_{term}[1 - \exp(-t/\tau_{term})], \quad (3)$$

where $L_{term} = \alpha S_0 N_m k_{sb} / z k_{cl}$ is the terminal length and $\tau_{term} = L_{term} z / F_{c1}$ is the characteristic time for growth termination. Here $k_{cl} = A\exp(-E_{cl}/k_B T)$ and $k_{sb} = B\exp(-E_{sb}/k_B T)$ are the rate constants for carbonaceous layer formation and surface-bulk penetration, respectively with the corresponding activation energies E_{cl} and E_{sb}, and α is a fraction factor, N_m=3.82×10^{15} 1/cm^2 is an areal density of C, and z is the number of C per 1μm of CNT length. According to Eq. (3) the growth rate decreases exponentially with the initial growth rate, $v = F_{c1}/z$. In a simple approximation k_{sb} is identical to the rate constant of C diffusion through the nanoparticle, k_t, after penetration of the surface $k_t = k_{sb} = (D_0/R^2)\exp(-E_b/k_b T)$, where R is the radius of the nanoparticle, D_0 is the diffusion factor, and E_b is the activation energy. For example, in the case of iron nanoparticle $D_0 \approx 0.1$–0.5 cm^2/s and $E_b \approx 1.4$–1.6 eV, for the temperatures T = 1000–1500K.[30] The same functional form, derived empirically has been used by Futaba et al. to fit the time dependences of single wall carbon nanotube arrays heights in the case of water-assisted growth, so-called "supergrowth" by the authors.[31] In the simplest case of SWNTs grown using Ni and Co catalysts and ethanol vapor as a feedstock, predictions of the model were verified using *in situ* Raman monitoring.[12] It has been confirmed that in the

low temperature limit the growth rate and the terminal time follow an exponential dependence with $v \propto F_{c1}$, and $\tau_{term} \propto 1/F_{c1}$.[12] Another experiment, which involved growth of SWNT arrays using a Co/Mo catalyst and ethanol vapor as CVD gas, and *in situ* absorption monitoring, also confirmed the main predictions of this model including the linear dependence on the feedstock concentration below the optimum growth pressure.[8]

In the case of MWNTs comparison of the theory with experiments based on measuring of VANTA length requires knowledge of the factor z, which includes the number of nanotube walls. The number of C per 1 μm of CNT length depends on the nanotube radius, R, and the number of walls N_w [32]

$$z = 2\pi R N_m N_w [1 - (N_w - 1)\,\Delta R/2R]\,, \qquad (4)$$

where $\Delta R = 0.335$ nm is the interlayer spacing[32]. The key parameter here is the number of walls. It is important to include this parameter to describe growth kinetics of multiwall carbon nanotubes (MWNTs) based on VANTA height measurements, using the model outlined above.

Initially, to determine the number of walls we artificially introduced a "disordered layer" near the surface of a catalyst nanoparticle that channeled the C atoms to a nanotube growing from this nanoparticle. The thickness of this layer was

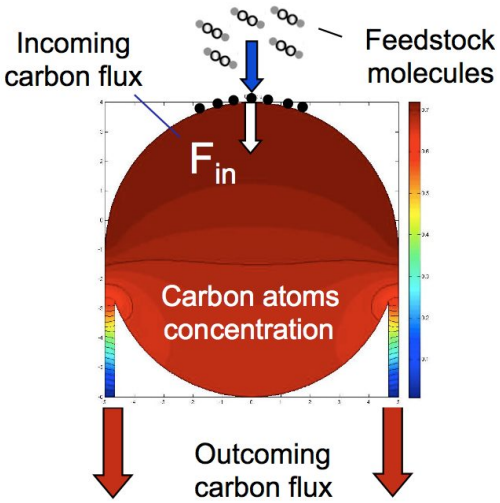

Figure 1. Diffusion of C atoms through a solid spherical carbon nanoparticle. The color bar shows the concentration of carbon in the nanoparticle (see Ref.32 for details.

determined by the total number of C atoms, processed by the catalyst nanoparticle at the specific growth conditions. This thickness, expressed in the number of carbon monolayers determined the number of walls that is proportional to the concentration of feedstock gas, n, (see Ref.[4] for details). Later we realized that the number of walls could be also determined within the frame of the common concept, i.e., dissociation of the feedstock gas on a catalyst nanoparticle surface, followed by diffusion of C-atoms into and through the bulk and along the surface of the nanoparticle to the sites where the nanotube grows (Fig.1). The details of this approach are described in Ref.[32]. Here we will give only the main idea and discuss the final results for the number of walls as a function of the temperature and feedstock gas pressure. The number of walls is determined by the interplay of the incident flux of atomic carbon and the diffusion rate and can be expressed in terms of optimal SWNT flux, i.e., the flux, F_{sw}, required to grow a SWNT at the maximum rate under the given conditions (Fig.2). In the simplest case

$$N_w \approx G\, F_{in}/F_{SW}\,, \qquad (5)$$

where G is a constant (Fig. 1). The outcoming flux, that is optimal for SWNT growth is the specific characteristic of a catalyst nanoparticle and can be estimated as

$$F_{SW} \approx CD_0(T)T^{1/2}\exp\left[-(E_{a1}+E_b)/k_BT\right], \quad (6)$$

where C is a constant, and $F_{in}(T) = F_{c1}$.[32] From Eqs. (5) and (6) one can see that

$$N_w \propto n\exp(E_B/k_BT) \quad (7)$$

This is an important result, and it allows one to use Eq. (3) to predict the growth rates and the termination times at low temperatures when "high temperature poisoning" can be neglected and MWNTs can be grown. In the case of SWNTs this estimate is straightforward since $N_w = 1$.

As it can be seen in Fig. 2, the number of walls can be controlled by adjusting the supply of carbon, and indeed SWNTs grow at the temperature corresponding to the crossover point between F_{in} and F_{sw} (T~700 °C). At lower temperatures ($T < 700$ °C) carbon is oversupplied, the diffusion rate through the nanoparticle is insufficient to process it, and the nanoparticle responds by supporting more walls. Conversely, at higher temperatures ($T > 700$ °C) carbon is undersupplied, the diffusion rate through the nanoparticle is sufficient to process it, and the particle responds by

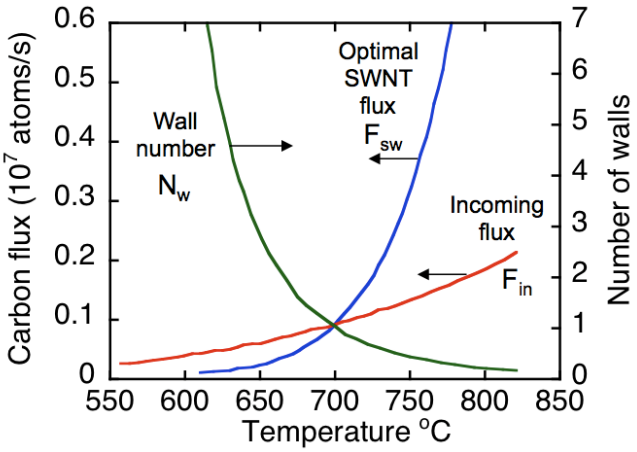

Figure 2. Carbon fluxes through a catalyst nanoparticle and the number of walls as a function of temperature. (Ref. 32)

supporting a single wall. But of coarse, in experiments we never have a situation when the growth rate increases exponentially with the temperature. Usually, in our experiments the growth rate drops rapidly when the temperature increases above 700 °C.[4]

Now we can consider predictions of the simplest version of the kinetic model, described by Eq. (3), for the case of MWNTs. We have shown that Eq. (3) describes well the length of MWNT arrays as a function of time in the low-temperature regime (T<700 °C).[4] The model also predicts that in the case of MWNT arrays, the growth rate at low temperatures is

$$v = F_{c1}/z \propto F_{c1}/N_w \propto \exp[-(E_{a1}+E_b)/k_BT], \quad (8)$$

and does not depend on the partial pressure of the feedstock gas. This is exactly what we observed in the range of C_2H_2 flows from 2 to 19 sccm for a growth temperature of 575 °C (see Ref. 4). Also confirmed in those experiments was the prediction that the terminal length of the MWNT arrays was inversely proportional to the partial density of feedstock molecules in the gas flux – i.e., $L_{term} \propto 1/n$.[4]

To account for a noted drop in the growth rate at the higher temperatures, we introduced a "high temperature poisoning" term to the rate equations, which contained only one additional rate constant with a corresponding activation energy, $E_p \approx 2.6\ eV$ (see Ref. 4). By doing this we were able to fit the observed temperature dependences of the growth rate, thereby explaining the observed maxima and high temperature decrease in the growth rate and the terminal length.[4,32]

In a number of experimental studies, similar dependences of growth rate on temperature have been observed, and different catalysts and feedstock gases have used to derive the corresponding activation energies of the processes involved in the growth (see, for example the recent papers[8,12,14, 33-35] and Refs. therein). In some cases the derived numbers of the activation energies were used to figure out the main processes involved in the growth and they varied from 0.23 eV for plasma enhanced CVD[33] to 2.3 eV.[14] Some variations can be explained by completely different catalyst systems and feedstock gases used to grow nanotubes. In many cases Eq. (3) or similar functional forms have been used to derive the activation energies. However, it is important to note that interpretation of the activation energies based on Eq. (3) has some limitations. The first limitation is that it can be used only at low temperatures, $T < T_m$, where T_m is the temperature corresponding to the maximum of the growth rate. The second important point is that in the case of MWNT arrays interpretation of measured activation energies should take into account the temperature dependence of the number of walls (Eq.7).

Many experimental studies, especially those carried out with very low partial pressures of the feedstock gas, show S-shape kinetics in the L(t) curve with an induction time.[35-37] In some cases, including our work,[4,13] it was difficult to observe the initial nucleation stage due to the long time required for the feedstock gas to reach a substrate located typically at the center of a long quartz tube CVD reactor. For example, in the experiment described in Ref. 4 the actual growth starts approximately after 25 s after the release of C_2H_2. This delay was explained by considering the time required for C_2H_2 to reach a Si substrate at some point in the reactor. For the experimental geometry and flow rates used in our work, it was estimated to be ~ 20 s. The feedstock gas introduction front was described with a function, g(t), which took into account diffusion of the acetylene at the leading edge during propagation toward the substrate. However, molecular beam feedstock gas introduction used in Ref. 37 clearly showed flux dependent induction times in VANTA growth, and to explain the initial stages of nanotube growth a phenomenological kinetic model was developed that included an autocatalytic term in the rate equations.[38,39] Other interesting variations of kinetic models included consideration of detailed gas-phase reactions of feedstock gases and their products (see, for example, Ref. 40 and references therein).

One of the most important questions in carbon nanotube growth is growth termination. The mechanism of the growth termination is still unclear despite many experimental and theoretical efforts to understand it. To explain the experimental kinetics at different temperatures we have introduced two different termination terms to the kinetics equations describing so-called low- and high-temperature growth termination regimes[4]. In both cases the termination of the growth should follow an exponential time dependence similar to that described by Eq. (3), and in many cases, especially for relatively short SWNT arrays, this theory well-describes the experimental L(t) curves. But for long VANTAs in many cases a new phenomenon of sudden termination has been observed with *in situ* optical imaging, and in some cases pauses subsequently occur followed by retraction and local equilibration in length during growth.[13]

The abrupt growth termination has been investigated in several other works,[5,15,41-46] and different mechanisms have been proposed to explain the behavior. Stadermann et al.[41] and Wang et al.[42] simply modified the kinetics of the carbonaceous layer poisoning of a catalyst nanoparticle by modeling the accumulation of the amorphous carbon patches at the surface of the nanoparticle using Kolmogorov-Johnson-Mehl-Avrami theory. Mattevi et al. attributed this effect to a decreasing number of active catalyst nanoparticles.[43] Vinten et al. concluded that the abrupt termination is the collective phenomenon caused by buildup of strain in VANTAs as they grow.[15] Real-time kinetics measurements by Bedewy et al.[44] and Meshot et al.[5] revealed loss of alignment in VANTAs near the termination point. Amama et al.[45] and Hasegawa et al.[46] concluded that the size of catalyst nanoparticles increases with time due to Ostwald ripening, and that in the case of water assisted growth water inhibits the ripening and prolongs the growth.

New interesting results on the atomic-scale observation of carbon nanotube growth have been obtained recently using *in situ* environmental transmission electron microscopy (TEM),[23-25] and it was demonstrated that nanotubes grow from solid Fe_3C nanoparticles, when Fe nanoparticles were used as a catalyst and C_2H_2 as a feedstock gas. Gamalski et al. observed length instabilities in the growth of MWNTs, and also an interesting phenomenon of detachment of a growing nanotube from the catalyst nanoparticles followed by nucleation of a new nanotube.[23] To explain this effect they used a diffusion-precipitation model similar to that described above.[32] According to their model, the outer walls grow faster than the inner walls due to differences in surface diffusion rates of carbon compared to those in nanoparticle bulk. As a result, tension in the inner walls accumulates and finally the nanotube detaches from a catalyst nanoparticle.

3. MODEL PREDICTIONS: SWNT VERSUS MWNT GROWTH

To test how the number of walls responds to variations in carbon supply, we designed a simple experiment depicted in Fig. 3. The growth starts at very low partial pressures of C_2H_2 when SWNTs are expected to grow (tube 1 in Fig. 3), then the flow increases 10 fold to grow MWNTs (tube 2 in Fig. 3), and after that the C_2H_2 flow drops back to the initial low value of 0.6 sccm, where again SWNTs are supposed to grow. Tube 3 in Fig. 3 represents the expected case, SWNT/MWNT/SWNT, but in reality the tube to the far right is what resulted. The specific experiment was as follows: Using Fe (1nm)/ Mo(0.2 nm)/Al(10 nm) catalyst films, growth was started on a Si substrate using 0.6 sccm of C_2H_2 in flowing Ar (2000 sccm) and H_2 (400 sccm) at atmospheric pressure. The details of the CVD reactor, used for this experiments are described in Ref. 4, but note that after 10 min the C_2H_2 was stopped for 4 min, followed by growth for another 10 min with a C_2H_2 flow of 6 sccm. After that the C_2H_2 flow was again decreased to 0.6 sccm and nanotubes were allowed to grow for another 10 min. Figure 4a shows cross-sectional SEM images of the top and bottom sections of this nanotube array.

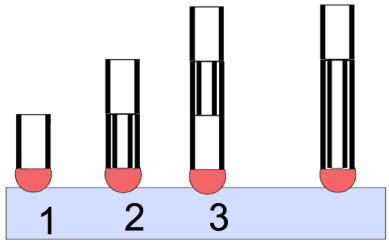

Figure 3. Switching the partial pressure of C_2H_2 gas during VANTAs growth, tubes 1-3 depict an expected outcome of the experiment. The tube at the right illustrates the result of this experiment.

To determine the single- versus multiwall VANTAs we measured Raman spectra of the cross-section along its length. Fig. 4b shows two spectra measured at the top and the bottom of the array at the positions shown by the colored dots in the SEM images. According to the Raman spectra (Fig. 4b, c), the first 50 μm of growth at the low partial pressure of C_2H_2 produces SWNTs. Then the growth switches to MWNTs when the partial pressure of C_2H_2 increases by the factor of ten in accordance with the model prediction. Surprisingly, when the feedstock pressure was switched back to the low value growth did not return to SWNTs and MWNTs continued to grow. This means that exposure of the catalyst nanoparticles to high fluxes of the feedstock gas changes the catalytic property of nanoparticles irreversibly in such a way that they cannot maintain the growth of SWNTs. The atomic nature of these changes remains unclear at this point. This experiment clearly demonstrated that the partial pressure of the feedstock gas is the important parameter to control the number of walls according to predictions of the model.

3. PULSED CVD APPROACH AND EXPERIMENTS

3.1 Pulsed CVD reactor

To further explore the growth kinetics we used fast pulsed feedstock gas introduction. In this approach short acetylene gas pulses of variable flux were injected into a low-pressure, high-velocity flow of Ar/H_2 to limit the feedstock gas pulse broadening due to diffusion. The main characteristics of our pulsed CVD reactor and the new effects in fast growth kinetics of VANTAs, revealed by pulsed growth and *in situ* time resolved reflectivity, are discussed below.

Figure 5 shows the schematic of our CVD reactor. To ensure fast delivery of the feedstock gas we injected a short pulse of acetylene from a pulsed valve into a fast continuous flow of Ar (2000 sccm) and H_2 (250 sccm). For pulsed growth, Ar (2000 sccm) and H_2 (250 sccm) were flowed continuously and acetylene was injected from a pulsed valves (*Parker* models: 099-0167-900 and 099-0340-900 with the orifice diameters of 3 and 0.8 mm, respectively). The pulsed

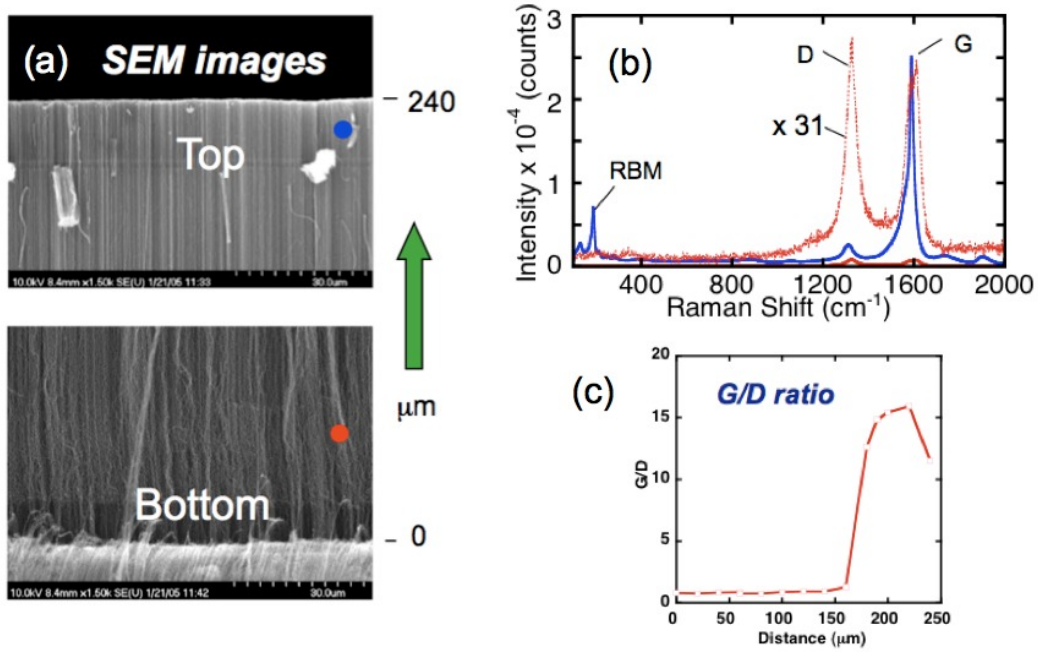

Figures 4a-c. (a) Cross-sectional SEM images of VANTAs measured at the top and the bottom of the arrays. (b) Raman spectra of the VANTAs measured at the points shown by colored dots in (a). (c) G/D ratio measured along the length of the array.

valve was actuated by a valve driver circuit which was triggered by a digital delay generator (Stanford Research Systems, SR545), and opened for a minimum time of 1 ms. The peak acetylene flux in a pulse could be varied by adjusting the backing gas pressure of acetylene to the valve, the duration of the trigger pulse, and by choosing a "small" or a "big" valves with a 0.8 or 3 mm orifices, respectively.

To understand the dynamics of the feedstock gas propagation, i.e., the arrival time to the substrate, as well as the shape and the width of the C_2H_2 pulses at the substrate location we performed modeling of the CVD reactor. Figure 6a shows the radial profiles of the temperature and the radial velocity at the center of the quartz tube at the Si-substrate location,

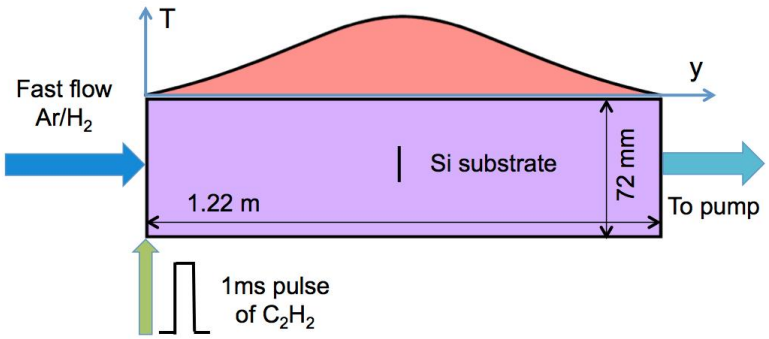

Figure 5. Schematic of a pulsed CVD reactor. Fast continuous flow of Ar/H_2 is introduced into a quartz tube trough mass-flow controllers at 2000/200 sccm, respectively. The other end of the tube is pumped down and the stationary pressure of about 6 Torr is maintained at this end. The feedstock gas, C_2H_2, is injected into the Ar/H_2 flow through a pulsed valve. A Si-substrate with catalyst films is placed in the center of the quartz tube. The curve at the top shows temperature profile along the walls of the quartz tube, which is varied from 300K at the ends to 1000K at the center of the tube, Ref. 47.

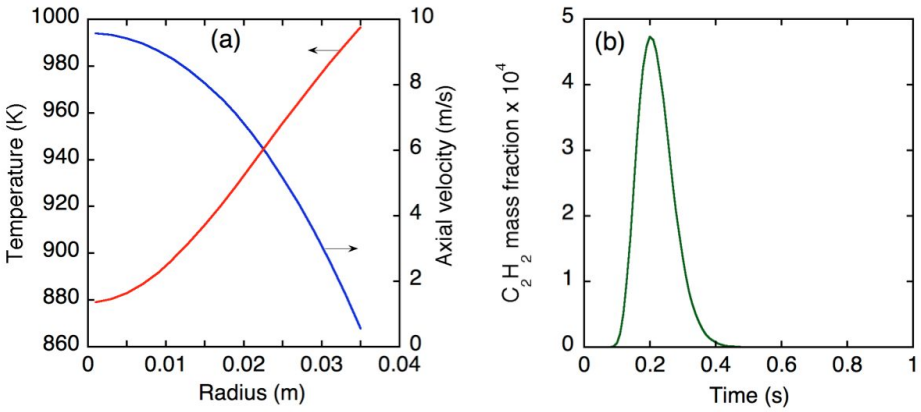

Figures 6a, b. (a) Radial profiles of the gas temperature and the axial velocity at the center of the quartz tube at t=0.2s after the valve was actuated. (b) Calculated shape of C_2H_2 gas pulse at the location of the substrate, Ref. 47.

and indicates that 0.2 s after the valve was opened, the C_2H_2 pulse maximum arrives.

One can see that the axial velocity at the center is very high, ~ 10 m/s. The temperature at the center of the quartz tube is about 880 K which is slightly lower than the maximum wall temperature of ~1000 K. The C_2H_2 gas pulse is relatively narrow (~120 ms FWHM) and has a sharp leading edge. The leading edge of the pulse arrives at the substrate at 100 ms after actuation of the valve, and peaks at 200 ms. More detailed characterization of the CVD reactor based on calculations of the gas dynamics, including 2D counter plots of the temperature, C_2H_2 gas concentration, and axial and radial velocities are described in Ref. 47. These calculations show that the shape and duration of the gas pulse will allow one to study fast nucleation and growth kinetics with times < 100 ms.

3.2 *In situ* measurements of pulsed growth kinetics

To grow VANTAs, using the approach described above, we used Si(100) wafer substrates with a 30 nm-buffer layer of Al_2O_3 and a Fe catalyst film nominally thickness 0.5 nm thick. The growth was monitored by time resolved reflectivity (TRR) (~ 3 ms time resolution) described in details in Ref. 4. The repetition rate of gas pulses was 0.1 Hz and the onset

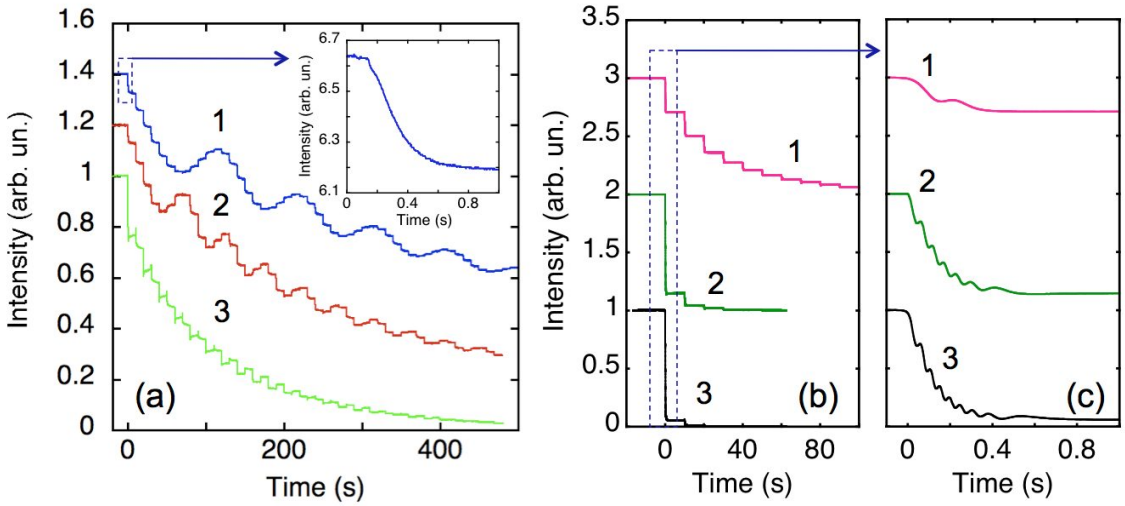

Figures. 7a-c. Intensity of the reflected light from a HeNe-laser (632.8nm) versus time measured at different backing pressures, using (a) a "small" valve[47] and (b, c) a "big" valve[48,49]. The curves 1-3 in (a-c) correspond to different backing pressures of 20, 40, and 60 psi, respectively. In all cases the growth temperature was 720 °C. The insert in (a) shows the magnified view of the first pulse for curve 1. The magnified view of the first pulses in (b) is shown in (c).

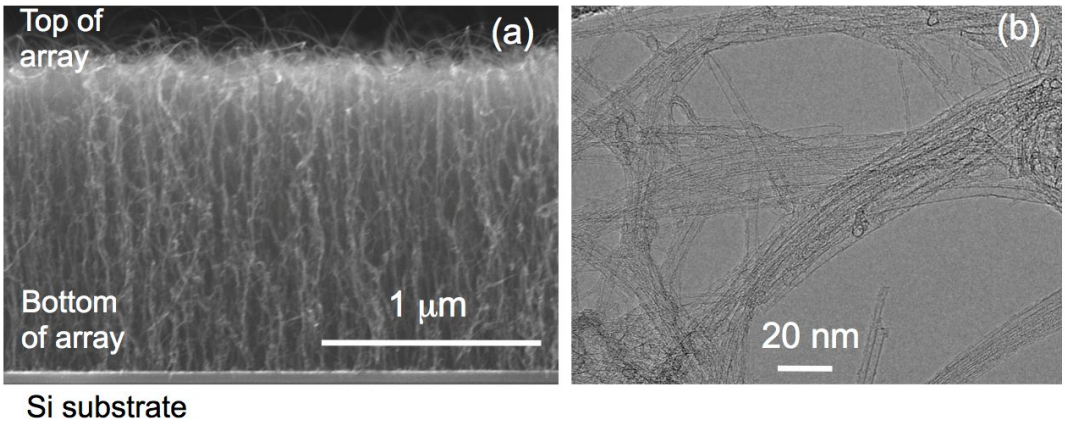

Fig. 8a, b. (a) Cross-sectional SEM and (b) TEM images of carbon nanotubes, grown using 55 pulses of C_2H_2 from a "small" valve at 720 °C and 20 psi backing pressure.

of valve opening was detected simultaneously with the TRR signal using a small piezoelectric microphone attached to the valve. The peak fluxes for each valve and the different backing pressures were calculated by measuring the C_2H_2 pressure rise per pulse in the evacuated CVD reactor at room temperature. The pressure per pulse was then converted to the standard cm^3/pulse using the known volume of the CVD reactor (5550 cm^3), and finally, to the peak flux in standard cubic centimeters per minute (sccm), assuming the duration of the gas pulse at the substrate of 120 ms FWHM (see Fig. 6b).

Figures 7a-c show *in situ* TRR signals obtained during pulsed growth of VANTAs, measured using different peak fluxes of C_2H_2. All curves show clear Fabry-Perot interference fringes, resulted from interference between light reflected from the top of the nanotube array and from the Si substrate.[2,4] In addition one can see small steps in the curves measured at low C_2H_2 peak fluxes corresponding to incremental growth of VANTAs.[47] For example, at the smallest peak flux of 60 sccm (curve 1 in Fig. 7a) it takes 12 C_2H_2 gas pulses to reach the first interference maximum corresponding to VANTA length of about 300 nm. The growth rate in this case is very low, ~25 nm/pulse. Figures 8a, b show cross-sectional SEM and TEM images of these nanotubes. According to TEM images this array contains mainly SWNTs with very small numbers of double wall nanotubes (<1%). At the highest peak flux of ~2000 sccm (curve 3 in Figs. 7b,c) we measured 8 fringes per the first pulse corresponding to 2.4 μm of VANTA length. In this case VANTAs grow very fast with the growth rates ~ 7μm/s.[48,49]

4. CONCLUSIONS

The recent development of our growth kinetic model and its applications for interpreting different nanotube growth experiments is reviewed. The simplest version of the model with an exponential decrease of the growth rate, Eq. (3), was used by many groups to fit kinetic data measured using *in situ* monitoring of the growth. Although, this model works well at relatively low temperatures for both SWNTs and MWNTs, we showed that in the case of MWNT arrays it is important to take into account the temperature dependence of the number of walls, Eq. (7), to correctly interpret the experimental activation energies measured from the corresponding Arrhenius plots. This also explains some variations of the activation energies in the literature.

The model also successfully explains the observed temperature dependences of the growth rate and the terminal length by including additional term that describes high temperature "poisoning" of catalyst nanoparticles. This approach naturally explains the variations in the activation energies and low and even zero activation energies measured at the higher growth temperatures (see for example, Ref. 12). The model also describes the number of walls as a function of the feedstock pressure and temperature and helped to interpret recent *in situ* HR TEM observations.[23]

However, the model does not explain the phenomenon of sudden growth termination, frequently observed in many works, especially in the case of long VANTAs. This is understandable since the model is based on considering of nanotube growth from a single nanoparticle, without taking into account collective effects that define alignment and can

also explain the abrupt growth termination, for example by buildup of strain in VANTAs as they grow.[15] We also introduced a pulsed growth approach, which allowed us to study fast growth kinetics as well as synthesize new VANTA architectures. The pulsed growth approach clearly demonstrated that SWNT VANTAs could be grown incrementally by pulsing the feedstock gas. The shortest nanotube array grown in our experiments was about 60 nm, but it should be noted that in this case the top surface of VANTAs was covered with randomly oriented nanotubes, which extend far above the 60 nm limit.[47] The multiple-pulse growth experiments (> 100 pulses with 0.1 Hz repetition rate) showed that a high fraction of nanotubes could be re-nucleated on the subsequent gas pulses (see also Ref. 47). In the case of the relatively low peak fluxes described in this paper, we did not notice any substantial changes in VANTAs morphologies related to stopping and starting the growth using extensive HR TEM characterization. However, the situation changes completely when the C_2H_2 flux increases, and in this case, nanotube arrays are comprised of individual bands with variable densities and orientations (see Refs. 48, 49).

An interesting result revealed by the pulsed gas introduction at low peak fluxes is the observation of a double-peak in the kinetics of the first gas pulse. This means that initial exposure of the catalyst nanoparticles changes their morphologies or phase, and that the subsequent growth occurs from these modified nanoparticles. It might be that initial carburization of the catalyst upon the first exposure to C_2H_2 pulse and formation of Fe_3C are responsible for this feature, as shown by Yoshida et al.[24, 25] and Gamalski et al.[23], using *in situ* HR TEM imaging. As a result, when the areal density of the active catalyst nanoparticles is low VANTAs do not grow, but instead randomly oriented carbon nanotube evolve. We have demonstrated that this behavior, i.e., cooperative versus random growth, can be predicted based on the observation of the first TRR curve.

Pulsed growth approach opens new interesting opportunities in VANTAs growth for practical applications as well as for understanding of their growth mechanism. Another interesting application of the combined optical diagnostics and kinetic modeling approach is understanding of growth mechanisms of graphene on metal catalyst films.[1]

ACKNOWLEDGMENTS

The synthesis science is sponsored by the Materials Sciences and Engineering Division, Office of Basic Energy Sciences, U.S. Department of Energy. Characterization science including Raman spectroscopy and SEM part of this research was performed at the Center for Nanophase Materials Sciences user facility, which is sponsored at Oak Ridge National Laboratory by the Scientific User Facilities (SUF) Division, U.S. Department of Energy.

REFERENCES

[1] Puretzky, A. A., Geohegan, D. B., Pannala, S., Rouleau, C. M., Regmi, M., Thonnard, N., Eres, G., "Real-time optical diagnostics of graphene growth induced by pulsed chemical deposition," Nanoscale 5, 6507–6517 (2013).
[2] Geohegan, D. B., Puretzky, A. A., Ivanov, I. N., Jesse, S., Eres, G., Howe, J. Y., "In situ growth rate measurements and length control during chemical vapor deposition of vertically aligned multiwall carbon nanotubes," Appl. Phys. Lett. 83, 1851-1853 (2003).
[3] Kim, D. H., Jang, H. S., Kim, C. D., Cho, D. S., Yang, H. S., Kang, H. D., Min, B. K., Lee, H. R., "Dynamic growth rate behavior of a carbon nanotube forest characterized by in situ optical growth monitoring," Nano Lett. 3, 863-865 (2003).
[4] Puretzky, A. A., Geohegan, D. B., Jesse, S., Ivanov, I. N., Eres, G., "In situ measurements and modeling of carbon nanotube array growth kinetics during chemical vapor deposition," Appl. Phys. A-Mater. 81, 223-240 (2005).
[5] Meshot, E. R., Hart, A. J., "Abrupt self-termination of vertically aligned carbon nanotube growth," Appl. Phys. Lett. 92, 113107 (2008).
[6] Murakami, Y., Miyauchi, Y., Chiashi, S., Maruyama, S., "Direct synthesis of high-quality single-walled carbon nanotubes on silicon and quartz substrates," Chem. Phys. Lett. 377, 49-54 (2003).
[7] Maruyama, S., Einarsson, E., Murakami, Y., Edamura, T., "Growth process of vertically aligned single-walled carbon nanotubes," Chem. Phys. Lett. 403, 320-323 (2005).
[8] Einarsson, E., Murakami, Y., Kadowaki, M., Maruyama, S., "Growth dynamics of vertically aligned single-walled carbon nanotubes from in situ measurements," Carbon 46, 923-930 (2008).
[9] Chiashi, S., Murakami, Y., Miyauchi, Y., Maruyama, S., "Cold wall CVD generation of single-walled carbon nanotubes and in situ Raman scattering measurements of the growth stage," Chem. Phys. Lett. 386, 89-94 (2004).

[10] Kaminska, K., Lefebvre, J., Austing, D. G., Finnie, P., "Real-time in situ Raman imaging of carbon nanotube growth," Nanotechnology 18, 165707 (2007).
[11] Finnie, P., Li-Pook-Than, A., Lefebvre, J., "The Dynamics of the Nucleation, Growth and Termination of Single-Walled Carbon Nanotubes from in situ Raman Spectroscopy During Chemical Vapor Deposition," Nano Res. 2, 783-792 (2009).
[12] Picher, M., Anglaret, E., Arenal, R., Jourdain, V., "Self-Deactivation of Single-Walled Carbon Nanotube Growth Studied by in Situ Raman Measurements," Nano Lett. 9, 542-547 (2009).
[13] Puretzky, A. A., Eres, G., Rouleau, C. M., Ivanov, I. N., Geohegan, D. B., "Real-time imaging of vertically aligned carbon nanotube array growth kinetics," Nanotechnology 19, 055605 (2008).
[14] Vinten, P., Lefebvre, J., Finnie, P., "Kinetic critical temperature and optimized chemical vapor deposition growth of carbon nanotubes," Chem. Phys. Lett. 469, 293-297 (2009).
[15] Vinten, P., Marshall, P., Lefebvre, J., Finnie, P., "Distinct termination morphologies for vertically aligned carbon nanotube forests," Nanotechnology 21, 035603 (2010).
[16] Helveg, S., Lopez-Cartes, C., Sehested, J., Hansen, P. L., Clausen, B. S., Rostrup-Nielsen, J. R., Abild-Pedersen, F., Norskov, J. K., "Atomic-scale imaging of carbon nanofibre growth," Nature 427, 426-429 (2004). J.
[17] Rodriguez-Manzo, A., Terrones, M., Terrones, H., Kroto, H. W., Sun, L. T., Banhart, F., "In situ nucleation of carbon nanotubes by the injection of carbon atoms into metal particles," Nature Nanotechnol. 2, 307-311 (2007).
[18] Lin, M., Tan, J. P. Y., Boothroyd, C., Loh, K. P., Tok, E. S., Foo, Y. L., "Direct observation of single-walled carbon nanotube growth at the atomistic scale," Nano Lett. 6, 449-452 (2006).
[19] Sharma R., Iqbal, Z., "In situ observations of carbon nanotube formation using environmental transmission electron microscopy," Appl. Phys. Lett. 84, 990-992 (2004).
[20] Sharma, R., Rez, P., Brown, M., Du, G. H., Treacy, M. M. J., "Dynamic observations of the effect of pressure and temperature conditions on the selective synthesis of carbon nanotubes," Nanotechnology 18 (12), 125602 (2007).
[21] Sharma, R., Rez, P., Treacy, M. M. J., Stuart, S. J., "In situ observation of the growth mechanisms of carbon nanotubes under diverse reaction conditions," J. Electron. Microsc. 54, 231-237 (2005).
[22] Sharma, R., Moore, E., Rez, P., Treacy, M. M. J., "Site-Specific Fabrication of Fe Particles for Carbon Nanotube Growth," Nano Lett. 9, 689-694 (2009).
[23] Gamalski, A., Moore, E. S., Treacy, M. M. J., Sharma, R., Rez, P., "Diffusion-gradient-induced length instabilities in the catalytic growth of carbon nanotubes," Appl. Phys. Lett. 95, 233109 (2009).
[24] Yoshida, H., Takeda, S., Uchiyama, T., Kohno, H., Homma, Y., "Atomic-scale in-situ observation of carbon nanotube growth from solid state iron carbide nanoparticles," Nano Lett. 8, 2082-2086 (2008).
[25] Yoshida, H., Shimizu, T., Uchiyama, T., Kohno, H., Homma, Y., Takeda, S., "Atomic-Scale Analysis on the Role of Molybdenum in Iron-Catalyzed Carbon Nanotube Growth," Nano Lett. 9, 3810-3815 (2009).
[26] Baker, R. T. K., Barber, M. A., Waite, R. J., Harris, P. S., Feates, F. S., "Nucleation and Growth of Carbon Deposits from Nickel Catalyzed Decomposition of Acetylene," J. Catal. 26, 51 (1972).
[27] Alstrup, I., "A New Model Explaining Carbon-Filament Growth on Nickel, Iron, and Ni-Cu Alloy Catalysts," J. Catal. 109, 241-251 (1988).
[28] Safvi, S. A., Bianchini, E. C., Lund, C. R. F., "The Dependence of Catalytic Carbon-Filament Growth-Kinetics Upon Gas-Phase Carbon Activity," Carbon 29, 1245-1250 (1991).
[29] Chitrapu, P., Lund, C. R. F., Tsamopoulos, J. A., "A Model for the Catalytic Growth of Carbon Filaments," Carbon 30, 285-293 (1992).
[30] Louchev, O. A., Laude, T., Sato, Y., Kanda, H., "Diffusion-controlled kinetics of carbon nanotube forest growth by chemical vapor deposition," J. Chem. Phys. 118, 7622-7634 (2003).
[31] Futaba, D. N., Hata, K., Yamada, T., Mizuno, K., Yumura, M., Iijima, S., "Kinetics of water-assisted single-walled carbon nanotube synthesis revealed by a time-evolution analysis," Phys. Rev. Lett. 95, 056104 (2005).
[32] Wood, R. F., Pannala, S., Wells, J. C., Puretzky, A. A., Geohegan, D. B., "Simple model of the interrelation between single- and multiwall carbon nanotube growth rates for the CVD process," Phys. Rev. B 75, 235446 (2007).
[33] Hofmann, S., Ducati, C., Robertson, J., Kleinsorge, B., "Low-temperature growth of carbon nanotubes by plasma-enhanced chemical vapor deposition," Appl. Phys. Lett. 83, 135-137 (2003).
[34] Bronikowski, M. J., "Longer nanotubes at lower temperatures: The influence of effective activation energies on carbon nanotube growth by thermal chemical vapor deposition," J. Phys. Chem. C 111, 17705-17712 (2007).
[35] Finnie, P., Li-Pook-Than, A., Lefebvre, J., "Phases of Carbon Nanotube Growth and Population Evolution from in Situ Raman Spectroscopy during Chemical Vapor Deposition," J. Phys. Chem. C 114, 11018-11025 (2010).

[36] Eres, G., Kinkhabwala, A. A., Cui, H. T., Geohegan, D. B., Puretzky, A. A., Lowndes, D. H., "Molecular beam-controlled nucleation and growth of vertically aligned single-wall carbon nanotube arrays," J. Phys. Chem. B 109, 16684-16694 (2005).
[37] Eres, G., Rouleau, C. M., Yoon, M., Puretzky, A. A., Jackson, J. J., Geohegan, D. B., "Model for Self-Assembly of Carbon Nanotubes from Acetylene Based on Real-Time Studies of Vertically Aligned Growth Kinetics," J. Phys. Chem. C 113, 15484-15491 (2009).
[38] Resasco, D. E., Monzon, A., Lolli, G., Cosma, S., Mohamed, S. B., "Kinetic Modeling of the SWNT Growth by CO Disproportionation on CoMo Catalysts," J. Nanosci. Nanotech. 8, 6141-6152 (2008).
[39] Monzon, A., Latorre, N., Romeo, E., Cazana, F., Ubieto, T., Royo, C., Villacampa, J. J., "Carbon Nanotube Growth by Catalytic Chemical Vapor Deposition: A Phenomenological Kinetic Model," J. Phys. Chem. C 114, 4773-4782 (2010).
[40] Pan, L. J., Ma, H., Nakayama, Y., "Modelling the growth of carbon nanotubes produced by chemical vapor deposition," Carbon 49, 854-861 (2011).
[41] Stadermann, M., Sherlock, S. P., In, J.-B., Fornasiero, F., Park, H. G., Artyukhin, A. B., Wang, Y. M., De Yoreo, J. J., Grigoropoulos, C. P., Bakajin, O., Chernov, A. A., Noy, A., "Mechanism and Kinetics of Growth Termination in Controlled Chemical Vapor Deposition Growth of Multiwall Carbon Nanotube Arrays," Nano Lett. 9, 738-744 (2009).
[42] Wang, X. Z., Feng, Y., Unalan, H. E., Zhong, G. F., Li, P., Yu, H., Akinwande, A. I., Milne, W. I., "The mechanism of the sudden termination of carbon nanotube supergrowth," Carbon 49, 214-221 (2011).
[43] Mattevi, C., Wirth, C. T., Hofmann, S., Blume, R., Cantoro, M., Ducati, C., Cepek, C., Knop-Gericke, A., Milne, S.C., Castellarin-Cudia, C, Dolafi, S., Goldoni, A., Schloegl, R., Robertson, J., "In-situ X-ray photoelectron spectroscopy study of catalyst-support interactions and growth of carbon nanotube forests," J. Phys. Chem. C 112, 12207-12213 (2008).
[44] Bedewy, M., Meshot, E. R., Guo, H., Verploegen, E. A., Lu, W., Hart, A. J., "Collective Mechanism for the Evolution and Self-Termination of Vertically Aligned Carbon Nanotube Growth," J. Phys. Chem. C 113, 20576-20582 (2009).
[45] Amama, P. B., Pint, C. L., McJilton, L., Kim, S. M., Stach, E. A., Murray, P. T., Hauge, R. H., Maruyama, B., "Role of Water in Super Growth of Single-Walled Carbon Nanotube Carpets," Nano Lett. 9, 44-49 (2009).
[46] Hasegawa, K., Noda S., "Millimeter-Tall Single-Walled Carbon Nanotubes Rapidly Grown with and without Water," ACS Nano 5, 975-984 (2011).
[47] Puretzky, A. A., Geohegan, D. B., Jackson, J. J., Pannala, S., Eres, G., Rouleau, C. M., More, K. L., Thonnard N., Readle, J. D., "Incremental Growth of Short SWNT Arrays by Pulsed Chemical Vapor Deposition," Small 8, 1534– 1542 (2012).
[48] Jackson, J. J., Puretzky, A. A., More, K. L., Rouleau, C. M., Eres, G., Geohegan, D. B., "Pulsed Growth of Vertically Aligned Nanotube Arrays with Variable Density," ACS Nano 4, 7573-7581 (2010).
[49] Geohegan, D. B., Puretzky, A. A., Jackson, J. J., Rouleau, C. M., Eres G., More, K. L., "Flux-Dependent Growth Kinetics and Diameter Selectivity in Single-Wall Carbon Nanotube Arrays," ACS Nano 5, 8311–8321 (2011).